Vulnerability of progeroid smooth muscle cells to biomechanical forces is mediated by MMP13

Patricia R. Pitrez[1,2], Luís Estronca[1,2], Luís Monteiro[1], Guillem Colell[3], Helena Vazão[1], Deolinda Santinha[1,2], Karim Harhouri[4], Daniel Thornton[5], Claire Navarro[6], Anne-Laure Egesipe[7], Tânia Carvalho[8], Rodrigo L. dos Santos[9], Nicolas Lévy[4], James C. Smith[10], João Pedro de Magalhães[1,5], Alessandro Ori[11], Andreia Bernardo[10], Annachiara De Sandre-Giovannoli[4], Xavier Nissan[7], Anna Rosell[3], Lino Ferreira[1,2]*

Affiliations:

[1]Center for Neuroscience and Cell Biology, University of Coimbra, Coimbra, Portugal

[2]Faculty of Medicine, University of Coimbra, 3000-548, Coimbra, Portugal

[3]Neurovascular Research Laboratory. Vall d'Hebron Research institute. Passeig Vall d'Hebron 119-129, 08035, Barcelona, Spain

[4]Molecular Genetics Laboratory, Department of Medical Genetics, La Timone Children's hospital, Marseille, France

[5]Integrative Genomics of Ageing Group, Institute of Ageing and Chronic Disease, University of Liverpool, Liverpool L7 8TX, United Kingdom

[6]Aix Marseille Univ, INSERM, GMGF, Marseille, France

[7]CECS, I-STEM, AFM, Institute for Stem Cell Therapy and Exploration of Monogenic diseases, Evry cedex, France

[8]IMM, Instituto de Medicina Molecular, Universidade de Lisboa, Lisbon, Portugal

[9]Cambridge Science Park, Mogrify Ltd, 25 Milton Road, Cambridge, CB4 0FW, UK

[10]Developmental Biology Laboratory, The Francis Crick Institute, London, NW1 1AT UK

[11]Leibniz Institute on Aging-Fritz Lipmann Institute, 07745 Jena, Germany

*Correspondence to: lino@uc-biotech.pt

Keywords: Progeria, aging, disease modelling, induced pluripotent stem cells, therapies

Abstract

Hutchinson-Gilford Progeria Syndrome (HGPS) is a premature aging disease in children that leads to early death. Smooth muscle cells (SMCs) are the most affected cells in HGPS individuals, although the reason for such vulnerability remains poorly understood. In this work, we develop a microfluidic chip formed by HGPS-SMCs generated from induced pluripotent stem cells (iPSCs), to study their vulnerability to flow shear stress. HGPS-iPSC SMCs cultured under arterial flow conditions detach from the chip after a few days of culture; this process is mediated by the up-regulation of metalloprotease 13 (MMP13). Importantly, double mutant $Lmna^{G609G/G609G}Mmp13^{-/-}$ mice or $Lmna^{G609G/G609G}Mmp13^{+/+}$ mice treated with a MMP inhibitor show lower SMC loss in the aortic arch than controls. MMP13 up-regulation appears to be mediated, at least in part, by the up-regulation of glycocalyx. Our HGPS-SMCs chip represents a platform for developing treatments for HGPS individuals that may complement previous pre-clinical and clinical treatments.

Introduction

HGPS is caused by a single mutation in the lamin A/C gene (*LMNA*), resulting in the generation of an abnormal lamin A precursor named progerin [1,2]. One of the key reasons of premature death is the loss of smooth muscle cells (SMCs) in the medial layer of large arteries, followed by the appearance of collagen and extracellular matrix and the development of a severe arteriosclerotic process that leads to increased arterial stiffness [3-5]. The reasons of SMC loss remain to be determined. It has been suggested that this may happen due to pathophysiological changes inherent to prelamin A/progerin accumulation, such as the acceleration of vascular calcification via the activation of the DNA damage response and senescence-associated secretory phenotypes in vascular SMCs [6] or the downregulation of PARP1 [7]. It has also been shown that the combined effect of progerin accumulation and mechanical stress in mouse SMCs overexpressing progerin promoted cell detachment and death, while the disruption of the linker between nucleoskeleton and cytoskeleton complex ameliorated the toxic effects of progerin [8]. Neither of these studies have fully addressed the reasons behind SMC detachment and thus which therapeutic approach could be effective to prevent SMC loss.

iPSCs offer an unlimited source of SMCs to study HGPS. Recent studies have generated iPSCs from fibroblasts obtained from individuals with HGPS (hereafter referred to as HGPS-iPSCs) [9-11]. Strikingly, HGPS-iPSCs show low lamin A/C and progerin protein expression in the pluripotent state. However, the expression of progerin is reactivated after HGPS-iPSC differentiation into SMCs [7,9]. The differentiated cells show nuclear dysmorphology, cell growth retardation, susceptibility to apoptosis, proliferation reduction and DNA-repair defects; however, SMC performance under flow conditions has not been evaluated.

In this work, we develop an in vitro cell system comprising SMCs derived from HGPS-iPSCs cultured under flow conditions in a microfluidic device. We identify MMP13 as a mediator of SMC detachment using chemical and genetic assays. The generated double mutant

Lmna$^{G609G/G609G}$*Mmp13*$^{-/-}$ mice show an increase in SMCs in the aortic arch and a decrease in progerin-positive cells. Additionally, the inhibition of MMP13 in Lmna$^{G609G/G609G}$ mice by Batimastat, a drug that has been previously tested in clinical trials in cancer patients, reduces SMC loss. The results present here open perspectives for HGPS treatment.

Results

SMCs derived from HGPS-iPSCs are functional and share similar features to progerin-expressing cells

iPSCs were generated from HGPS skin fibroblasts and characterized as previously described [10]. iPSCs generated from non-disease cells (N-iPSCs), HGPS skin fibroblasts and non-disease somatic human vascular smooth muscle cells (hVSMCs) were used as controls. The mutation in the *LMNA* gene, both in HGPS skin fibroblasts and HGPS-iPSCs, was confirmed by Sanger sequencing (Supplementary Fig. 1). As expected, undifferentiated HGPS-iPSCs expressed low levels of HGPS markers, such as *progerin*, as well as low levels of SMC markers, such as *α-SMA* and *SMα-22* [12,13] (Supplementary Fig. 2a). To induce the differentiation of HGPS-iPSCs or N-iPSCs into SMCs, CD34$^+$ cells were isolated by magnetic-activated cell sorting from embryoid bodies cultured for 10 days in suspension (Fig. 1a) [14]. At this stage, HGPS-CD34$^+$ cells already express higher levels of progerin mRNA transcripts relative to N-iPSCs but relatively low levels of SMC mRNA transcripts compared to somatic hVSMCs (Supplementary Fig. 2b). HGPS-CD34$^+$ cells were then cultured in SMC induction media (Supplementary Fig. 3) followed by SMC maturation media (Supplementary Fig. 4) for an additional 4 passages. Matured SMCs are referred to as HGPS-iPSC SMCs or N-iPSC SMCs based on their phenotype, genotype and functional properties (see below). Both HGPS-iPSC SMCs and N-iPSC SMCs have similar or higher expression of SMC mRNA transcripts than somatic hVSMCs (Supplementary Fig. 4a). Greater than 95% of both differentiated cells express α-SMA, smooth muscle myosin heavy chain (SMMHC) and calponin proteins (Fig. 1b). Moreover,

HGPS-iPSC SMCs express progerin mRNA transcripts (Fig. 1c) and progerin protein (Supplementary Fig. 4b and Supplementary Fig. 4c). Similar results were obtained for SMCs derived from HGPS-iPSCs generated from a second Progeria individual; however, the differentiated cells showed higher progerin protein levels than the first Progeria individual (Supplementary Fig. 5). Importantly, HGPS-iPSC SMCs and N-iPSC SMCs are functional as they respond to vasoactive agents such as histamine and angiotensin (Supplementary Fig. 4d) and they contract after exposure to carbachol (Supplementary Fig. 4e).

SMCs derived from HGPS-iPSCs share similar features to progerin-expressing cells. Cell lines forced to express progerin show the activation of several NOTCH signaling pathway effectors [15]. Indeed, our results showed that HGPS-iPSC $CD34^+$ cells had higher expression of NOTCH signaling pathway mRNA transcripts than N-iPSC $CD34^+$ cells (Supplementary Fig. 6). Mature HGPS-iPSC SMCs also expressed higher levels of NOTCH ligand and receptors than N-iPSC SMCs (Supplementary Fig. 6a). Additionally, HGPS-iPSC SMCs responded to farnesyltransferase inhibitors, as has been shown in other Progeria cell models [16-18]. In the current work, HGPS-iPSC SMCs treated with lonafarnib for 48 h accumulated nuclear prelamin A and showed a decrease in nuclear shape abnormalities and nuclear blebbing (Supplementary Fig. 7a-c). Taken together, the cells differentiated from HGPS-iPSCs expressed SMC and progeroid markers, are functional and exhibit physiological responses.

HGPS-iPSC SMCs are vulnerable to arterial shear stress

SMCs differentiated from N-iPSCs or HGPS-iPSCs were seeded in a microfluidics system and cultured under flow conditions for up to 7 days (Fig. 1d). Because SMCs from large arteries are the most affected in blood vessels in HGPS, we used a flow of 20 dyne/cm^2, which is typically found in arterial blood vessels [19]. N-iPSC SMCs (Fig. 1g), hVSMCs or HGPS-Fibroblasts (80% of which

express progerin) (Fig. 1e,g) can be cultured in the microfluidics system for at least 7 days without a visible loss in cell number. In contrast, HGPS-iPSC SMCs cultured under flow conditions formed cell clumps overtime (Fig. 1f), and most of the cells detached from the substrate at day 4 as confirmed by cell number (Fig. 1g) and metabolic analyses (Fig. 1h). During this time period, the percentage of cells expressing progerin and displaying nuclear abnormalities increased significantly until day 4 (Supplementary Fig. 8). Our results indicate that SMC detachment is mediated by progerin accumulation, as the inhibition of progerin by antisense morpholinos [20] significantly decreased HGPS-iPSC SMC detachment (Supplementary Fig. 9). In addition, we showed that HGPS-iPSC SMCs with high progerin expression (30% of the cells express progerin at day 0) detached from the surface of the microfluidics system in a short time (<12 h) (Supplementary Fig. 5g). To confirm that progerin accumulation is responsible for SMC loss, a frameshift mutant stem cell line was generated (HGPSΔ2-iPSCs) to knockout the HGPS mutant allele and generated a disease cell line, as previously described in the mouse [21] (Fig. 2a and Supplementary Fig. 10). Specifically, a two-base pair deletion on exon 11, upstream of the HGPS point mutation (1814C>T), was generated. Notably, HGPSΔ2-iPSCs expressed little or no progerin upon differentiation into SMCs as demonstrated at the transcript and protein levels and did not detach under flow culture conditions (Fig. 2).

HGPS-iPSC SMC detachment does not seem to be mediated by cell apoptosis. Before cell detachment, HGPS-iPSC SMCs showed: (i) poor proliferation (as monitored by Ki67 staining) confirming their contractile phenotype (Fig. 1i), (ii) similar levels of apoptosis as N-iPSC SMCs as confirmed by caspase 9 activity (Fig. 1j), (iii) an osteogenic differentiation program (Supplementary Fig. 11a,b), (iv) increased DNA damage [6] (Supplementary Fig. 12) and (v) downregulation of NOTCH [15,22] (Supplementary Fig. 13) signaling pathways. Because the in vivo shear stress from blood flow is not directly sensed by SMCs but by endothelial cells (ECs), we co-cultured SMCs differentiated from HGPS-iPSCs (directly attached to the microfluidics substrate)

with human umbilical artery endothelial cells (HUAECs, on top of the SMCs) under flow conditions. Initially, we screened different culture conditions and we found that endothelial growth media-2 (EGM2) medium was a suitable medium to support both cells (Supplementary Fig. 14). Then, we co-cultured HUAECs and HGPS-iPSC SMCs at different ratios (1.6, 1 and 0.6) under flow conditions. In all the ratios tested, we had a monolayer of HUAECs (Supplementary Fig. 15a) and HGPS-iPSC SMCs at time zero. After 6 days in flow conditions, a significant percentage (>40%) of HGPS-iPSC SMCs was lost (Supplementary Fig. 15b). For the highest ratio tested (1.6), the loss of HGPS-iPSC SMCs occurred without visible loss of ECs. Yet, for EC:SMC ratios below 1, part of ECs also detached from the microfluidic chamber indicating that a low EC density may turn ECs vulnerable to flow conditions. Importantly, cell vulnerability to flow conditions was only observed in co-cultures of HGPS-iPSC SMCs but not N-iPSC SMCs (Supplementary Fig. 15c).

It has been shown that a knock-in mouse line carrying a homozygous Lmna c.1827C>T;p.Gly609Gly mutated allele (*Lmna*$^{G609G/G609G}$) recapitulates most of the described alterations associated with HGPS, including the loss of SMCs [20]. Thus, to validate the results obtained for the HGPS-iPSC SMCs, we isolated SMCs from wild-type (WT mSMC) and homozygous *Lmna*$^{G609G/G609G}$ (HOZ mSMC) mice. Both cells expressed calponin and α-SMA, while HOZ mSMCs, but not WT SMCs, showed dysmorphic nuclei and nuclear blebbing (Fig. 3a,b). WT mSMCs were cultured under flow conditions (120 dyne/cm^2 to mimic mice arterial flow shear stress [23,24]) for up to 26 days without visible loss of cells (Fig. 3c). In contrast, HOZ mSMCs detached from the substrate after 8-9 days. These results confirm that HOZ mSMCs are vulnerable to flow shear stress similar to HGPS-iPSC SMCs. Overall, our results indicate that HGPS-iPSC SMCs are vulnerable to flow shear stress, as in the case of SMCs isolated from mice carrying a HGPS-like mutation in the *Lmna* gene.

HGPS-iPSC SMCs have significant changes in extracellular matrix (ECM) secretion and MMP expression

To gain insights into the mechanism behind SMC detachment, we performed microarray analyses on HGPS-iPSC SMCs and N-iPSC SMCs at days 0 and 4 (before cell detachment). At day 0, 2084 genes were differentially expressed (Log2FC >=1; P < 0.05) in HPGS-iPSC SMCs *vs.* N-iPSC SMCs. Of these genes, 51 genes were associated with cell senescence, as determined by the intersection of all the differentially expressed genes with the CellAge database [25] (279 genes) (Supplementary Data 1). At the protein levels, HGPS-iPSC SMCs expressed higher levels of p21 and SA-β-galactosidase than N-iPSCs-SMCs and the level of senescence markers increased after culture of HGPS-iPSC SMCs in flow conditions (Supplementary Fig. 16a and Supplementary Data 5). We next performed pathway analysis on the differentially expressed genes from HGPS iPSC SMCs at day 0 *vs.* day 4 (Supplementary Fig. 17, Supplementary Data 2 and Supplementary Data 3). In general, ECM activation, secretion and cell adhesion pathways were up-regulated, whereas cell cycle and DNA replication pathways were down-regulated under arterial flow conditions at day 4. Among the 57 genes that were at least 3-fold down- or up-regulated compared to day 0 (p<0.001) (Fig. 4a), 5 were related to ECM secretion (*COL6A3, IBSP, BGN, SGCG, and EPPK1*) and 1 to metalloproteases (*MMP13*). The expression of these genes, as well as others, was confirmed by qRT-PCR (Fig. 4a), and the molecular network of genes that were differentially expressed between days 0 and 4 in the HGPS SMCs was examined by Ingenuity Pathway Analysis (Supplementary Fig. 17). Interestingly, pathway analysis suggested that *MMP13* is either a direct or indirect target of multiple genes upregulated at day 4. Moreover, *MMP13* transcript levels are elevated in HGPS-iPSC SMCs when compared to SMCs generated from the attenuated disease version of this line (HGPSΔ2-iPSC SMCs), specially post shear stress (Fig. 2g).

To further explore the gene array results, we evaluated whether the presence of ECM secreted by hVSMCs could prevent the detachment of HGPS-iPSC SMCs under arterial flow conditions. Thus,

we cultured HGPS-iPSC SMCs on decellularized ECM deposited by hVSMCs or directly on top of mitotically inactivated hVSMCs (Supplementary Fig. 18). Both conditions were unable to prevent HGPS-iPSC SMC detachment. Next, we tested whether conditioned media collected from HGPS-iPSC SMCs in flow conditions for 4 days could induce the detachment of flow shear stress-insensitive hVSMCs (Fig. 4b). Surprisingly, hVSMCs detach after perfusion with HGPS-iPSC SMC-conditioned media but not with N-iPSC SMC-conditioned media (Fig. 4c). Following these results and given that *MMP13* appears to be the downstream effector for the genes misregulated at day 4 (Supplementary Fig. 17b) we decided to quantify the concentration of MMP13 in HGPS-iPSC SMC and N-iPSC SMC culture media after flow shear stress. Remarkably, MMP13 levels increased 30-fold in the HGPS-iPSC SMC culture media, but not in the control cell culture media (Fig. 4d). Similarly, higher MMP13 levels were observed in media collected from HOZ mSMCs under flow shear stress, when compared to media from WT mSMCs (Fig. 3d). Because MMP13 is produced by cells as an inactive form (proMMP13), which is then activated by cell membrane MMPs, namely MMP14 (also called MT1-MMP) and MMP2 (also called gelatinase A) [26], the catalytic activity of MMP13 secreted by HGPS-iPSC SMCs was analyzed (Supplementary Fig. 19). The concentration of proMMP13 and active MMP13 increased approximately 8- and 5-fold, respectively, in culture media of HGPS-iPSC SMCs cultured in flow conditions from day 0 to day 4. Moreover, the concentration of proMMP13 and active MMP13 in cell culture media collected from N-iPSC SMCs cultured in flow conditions for 4 days was more than 4-fold lower than the one observed with HGPS-iPSC SMCs. Altogether, our results indicate that HGPS-iPSC SMCs cultured under flow conditions showed increased cell senescence, ECM activation, secretion and cell adhesion pathways up-regulation and dysregulation in the expression of MMP13.

MMP13 mediates HGPS-iPSC SMC loss under flow conditions

Next, we tested whether the chemical inhibition of MMPs could prevent HGPS-iPSC SMC detachment. For this purpose, we used Batimastat (BB-94) [27], a broad spectrum matrix metalloprotease inhibitor (IC50 = 33 nM for MMP13 [28]), and a specific MMP13 inhibitor pyrimidine-4,6-dicarboxylic acid, bis-(4-fluoro-3-methyl-benzylamide) (IC50= 8 nM) [29]. Remarkably, both inhibitors significantly decreased the detachment of HGPS-iPSC SMCs cultured under arterial flow conditions (at least until day 12) (Fig. 4e), and this effect was much superior to that of lonafarnib (Supplementary Fig. 7d) or inhibition through the pyrophosphate calcification process [30] (Supplementary Fig. 11c). To confirm these results, HGPS-iPSC SMCs were subjected to siRNA knockdown of MMP13 and cultured under arterial flow conditions for 10 days (Fig. 4f, g). Our results show that the knockdown of MMP13 in SMCs increased the stability of HGPS-iPSC SMCs in flow culture conditions compared to non-treated cells. We also analyzed the effects of MMP13 and BB94 inhibition in HOZ mSMCs (Fig. 3e). Similar to what was observed with HGPS-iPSC SMCs, the detachment was significantly delayed when one of the inhibitors was used. To further demonstrate the importance of MMP13 in HGPS-iPSC SMC detachment, we enforced the expression of *MMP13* in somatic SMCs (hVSMCs) and cultured the modified cells in flow culture conditions (Supplementary Fig. 19). Notably, the number of cells observed at day 7 is lower than the one observed in wild type cells indicating that some of the modified cells were lost during the flow culture conditions.

We then asked whether the modulation of MMP13 activity could affect progerin expression associated with the vulnerability of HGPS-iPSC SMCs to flow shear stress. Interestingly, chemical inhibition of MMP13 in HGPS-iPSC SMCs cultured for 7 days in flow conditions reduced the percentage of progerin-positive cells (Fig. 4h); however, it did not decrease progerin expression in cells with high levels of progerin, such as HGPS Fibroblasts. Additionally, the chemical inhibition of MMP13 did not reduce the activity of alkaline phosphatase in HGPS-iPSC SMCs cultured for 7 days in flow conditions (Fig. 4i). Overall, the results obtained after chemical and genetic inhibition,

the increase of MMP13 after flow shear stress and the effect of HGPS-iPSC SMC-conditioned media on cell detachment, indicate that MMP13 mediates SMC loss.

Inhibition of MMP13 in *Lmna*$^{G609G/G609G}$ mice significantly increased the number of SMCs in aortic arch

To confirm the importance of MMP13 dysregulation in progeroid animal models, we quantified MMP13 in the plasma of *Lmna*$^{G609G/G609G}$ and wild type mice (Fig. 5a). The results showed that the levels of MMP13 were higher in mutant mice (Fig. 5b). Then, we asked whether the inhibition of MMP13 in *Lmna*$^{G609G/G609G}$ mice could decrease SMC loss. For this purpose, we generated double mutant lines, *Lmna*$^{G609G/G609G}$*Mmp13*$^{-/-}$ and *Lmna*$^{G609G/G609G}$*Mmp13*$^{+/-}$ (Supplementary Fig. 20), and evaluated the heart rate and SMC loss in the aortic arch [20] of these mice at week 10 (Fig. 5a). Heart rate was chosen as a measure of the overall health status of the HGPS model and the derived double mutant lines, given that bradycardia was a clinical abnormality evidenced in both *Lmna*$^{G609G/G609G}$ mouse as well as Zmpste 24$^{-/-}$ progeria mouse models [20,31]. Both double mutant mice showed higher heart rates (Fig. 5d) and numbers of SMCs (Fig. 5c,e) in the aortic arch than *Lmna*$^{G609G/G609G}$ *Mmp13*$^{+/+}$ mice. Interestingly, *Lmna*$^{G609G/G609G}$*Mmp13*$^{-/-}$ and *Lmna*$^{G609G/G609G}$*Mmp13*$^{+/-}$ mice showed a lower number of progerin-positive cells in the aortic arch than non-mutated mice (Fig. 5c,f). In addition, *Lmna*$^{G609G/G609G}$*Mmp13*$^{+/-}$ mice (but not *Lmna*$^{G609G/G609G}$*Mmp13*$^{-/-}$ mice) showed an increase of the aortic media thickness being similar to the non-mutated mice (Fig. 6a), as confirmed by orcein staining. We performed proteomic analyses of aortic arches from mutated and non-mutated mice (n=>5 mice per strain) using data independent acquisition mass spectrometry [32,33]. Principal component analysis based on 2,260 proteins detected showed that the proteome profiles of aortic arches from *Lmna*$^{G609G/G609G}$*Mmp13*$^{+/-}$ mice were more closely related to the profile of wild type mice to that of *Lmna*$^{G609G/G609G}$ *Mmp13*$^{+/+}$ mice (Fig. 6c). From the 161 proteins differentially expressed between the mutant and wild type mice aortic arches ($q<0.05$ and abs($\log_2$

fold change)>0.58), approximately 25% of the proteins had similar expression in *Lmna*$^{G609G/G609G}$*Mmp13*$^{+/-}$ mice and wild type mice (Fig. 6c, Supplementary Data 4).

Motivated by these results, we then tested a therapeutic approach to reduce SMC loss in *Lmna*$^{G609G/G609G}$ *Mmp13*$^{+/+}$ mice. For this purpose, we used Batimastat because human safety has been previously demonstrated in clinical trials [34]. *Lmna*$^{G609G/G609G}$ *Mmp13*$^{+/+}$ mice at week 5 were intraperitoneal (IP) injected 5 times a week (Fig. 7a). At week 10, Batimastat-treated *Lmna*$^{G609G/G609G}$ *Mmp13*$^{+/+}$ mice had similar heart rates to non-treated animals (Fig. 7c); however, they showed higher SMCs in the aortic arch than non-treated mice, as confirmed by cell nuclei counts and verified by the increase levels of SMC markers determined by qRT-PCR analyses (Fig. 7b,d,e). No differences were observed between non-treated and Batimastat-treated mice regarding progerin accumulation in the aortic arch (Supplementary Figs. 20c). Overall, our data shows that the in vivo inhibition of MMP13 by genetic or chemical interventions yielded mice having significantly higher numbers of SMCs in the aortic arch.

Activation of MMP13 is mediated by the activation of the glycocalyx

The glycocalyx is a surface layer of proteoglycans and glycosaminoglycans that are immobilized in the cell membrane. Glycocalyx components have been shown to be involved in flow shear stress sensing by SMCs [35,36]. To identify the mechanism underlying the up-regulation of MMP13 in HGPS-iPSC-SMCs cultured under arterial flow, we analyzed glycocalyx gene mRNA transcripts (Fig. 8b). Interestingly, glycocalyx transcripts were up-regulated in HGPS-iPSC SMCs cultured under flow conditions for 4 days (Fig. 8b). From these upregulated genes, syndecan 2 gene (*SDC2*), which encodes the transmembrane (type I) heparan sulfate proteoglycan, was also upregulated in hVSMCs or N-iPSC SMCs cultured for 4 days in flow conditions (Supplementary Fig. 21). Because not all the glycocalyx mRNA transcripts were upregulated in hVSMCs and N-iPSC SMCs, the

results suggest that the composition of glycocalyx is likely different in these cells when compared to HGPS-iPSC SMCs. Next, we analyzed the expression of heparan sulfate at the protein level. In contrast to control cells, the expression of heparan sulfate increased when HGPS-iPSC SMCs were cultured under flow conditions (Fig. 8a). Importantly, the enzymatic cleavage of heparan sulfate by heparinase III (Supplementary Fig. 22) decreased MMP13 concentration in the cell culture media (Fig. 8c) and significantly decreased the detachment of HGPS-iPSC SMCs cultured under flow conditions (Fig. 8d). Moreover, the enzymatic cleavage of heparan sulfate slightly decreased alkaline phosphatase activity (Fig. 8e).

To further investigate a potential ECM target of MMP13 in SMCs, we monitored the expression of ECM components in hVSMCs, HUAECs, N-iPSC SMCs and HGPS-iPSC SMCs. Our results indicate that hVSMCs express higher levels of mRNA that encode collagen 1A1, collagen 3A1, collagen 4A2 and collagen 6A3 than HUAECs (Supplementary Fig. 21c). It has been shown that MMP13 degrades very efficiently the native helix of all fibrillary collagens, including collagen type I [37]. Our proteomic results indicate that indeed collagen 1A1 is upregulated in HGPS-iPSC SMCs exposed to flow conditions (Supplementary Fig. 16b) and thus it may be a potential target for MMP13. Overall, our results indicate that activation of MMP13 is mediated, at least in part, by glycocalyx activation.

Discussion

In this study, we developed a microfluidic chip formed by a monoculture or a co-culture of HGPS-SMCs (generated from iPSCs) with ECs to study the reason underlying HGPS-SMC vulnerability to flow shear stress. To generate the chip, we (i) developed a protocol to differentiate HGPS-iPSCs into functional HGPS-SMCs, (ii) demonstrated that HGPS-iPSC SMCs shared similar properties with other known progerin-expressing cells, (iii) confirmed that HGPS-iPSC SMCs were vulnerable

to arterial flow shear stress and (iv) validated the results in ex vivo SMCs isolated from *Lmna* $^{G609G/G609G}$ mice. Using the chip, we have identified MMP13 up-regulation as an important mediator of HGPS-SMC vulnerability to flow shear stress and we confirmed MMP13's role in vivo in *Lmna*$^{G609G/G609G}$ mice (Fig. 8f). MMP13 is up-regulated in a number of pathological states including atherosclerosis and rheumatoid arthritis [38]. The up-regulation of MMP13 in HGPS-SMCs cultured under arterial flow conditions is in line with examples in the literature showing that enzymatic ECM remodeling is significantly altered in HGPS cells [39-41].

Multiple protocols have been described in the literature for the differentiation of iPSCs into SMCs, either via an intermediate progenitor stage or directed differentiation [14,42-44]. These protocols are highly variable in terms of SMC differentiation efficiency, timescale and functionality (non-dividing contractile phenotype *versus* proliferative phenotype, secretory profile), likely due to the choice of precursor population to derive the SMC subtypes, the chemical composition of the differentiation medium, as well as the choice of inductive SMC factors (e.g. PDGF-BB, TGF-β1, retinoic acid). Three previous studies have reported the differentiation of HGPS iPSCs into SMCs [7,9,45] by direct differentiation [7] or by using an intermediate progenitor (i.e. mesenchymal stem cells [45] or $CD34^+$ cells [9]). In some cases, SMCs were not terminally differentiated (as confirmed by the expression of SMMHC) [7], in others the percentage of SMCs was relatively low (i.e. only 50-60% of the differentiated cells showed specific SMC markers including α-SMA, calponin 1 and SMMHC) [45] and no indication of SMC functionality [9] (e.g. contractility, intracellular accumulation of calcium after exposure to vasoactive agents) was reported. In the present study, we showed that the differentiation of HGPS-iPSCs induces the activation of the NOTCH signaling pathway, a hallmark of progerin-expressing cells [15]. This is observed in the $CD34^+$ progenitor cells and after their differentiation into SMCs. The $CD34^+$ cells have been reported to express KDR and CD31 [43] and, thus, are likely of lateral plate mesoderm origin [42,44]. Importantly, the differentiated cells express high levels of all the SMC markers analyzed (α-SMA, calponin and SMMHC), are contractile in

response to the muscarinic receptor agonist carbachol as observed in typical human aortic SMCs, and, when matured in culture for approximately 30 days, they express progerin. Therefore, our differentiation protocol compares favorably to other protocols in term of SMC yield and functionality. Interestingly, HGPS-iPSC SMCs express lower levels of calponin than in N-iPSC SMCs but the reason and possible implications behind this phenotypic difference remain to be determined. Nevertheless, most of the HGPS-iPSC SMCs expressed calponin at the protein level, both at the induction and maturation steps (Supplementary Figs. 3 and 4). A previous study has reported heterogeneous sized calponin 1-staining inclusion bodies in the cytoplasm of HGPS-SMCs [9]; however, such structures were not observed in the current study.

It has been reported that in wild type animals the aorta was one of the tissues with the highest expression of lamin A, while in progeroid animals the aorta was the first place where progerin was detected[8]. This explains the highest susceptibility of HGPS-SMCs located in the aorta to biomechanical forces. It has been reported that mouse SMCs overexpressing progerin exposed to biomechanical forces detach from the culture vessel after substrate stretching and die [8]. Yet, the mechanism of SMC detachment is still poorly understood. Our study indicates that MMP13 mediates SMC detachment as chemical or genetic inhibition of MMP13 reduces significantly SMC loss. In addition, we found that the accumulation of progerin is a mediator and not the cause of SMC detachment because HGPS Fibroblasts accumulate high levels of progerin and do not detach in flow conditions. Yet, both inhibition of progerin by morpholinos and the knockout of the HGPS mutant allele in HGPS-SMCs decreased or prevented SMC detachment in flow culture conditions.

Although $Lmna^{G609G/G609G}Mmp13^{+/-}$ and $Lmna^{G609G/G609G}Mmp13^{-/-}$ mice showed similar amelioration of SMCs loss in the aortic arch, our proteomic analyses in the same tissue showed that $Lmna^{G609G/G609G}Mmp13^{+/-}$ mice had a closer protein profile to wild type than $Lmna^{G609G/G609G}Mmp13^{-/-}$ mice. This was consistent with the media thickness size, which was more similar between wild type mice and $Lmna^{G609G/G609G}$ $Mmp13^{+/-}$ than to $Lmna^{G609G/G609G}$ $Mmp13^{+/+}$

mice. Previous studies have shown that *Mmp13*$^{-/-}$ mice had defects in vascularization [46] and thus the full deficiency of MMP13 in the aortic arch might not be desirable to establish a phenotype closer to the normality.

The accumulation of proteoglycans in Progeria mouse models [47] as well as in atherosclerotic lesions in HGPS individuals [5] has been demonstrated. According to our results, the up-regulation of MMP13 in HGPS-SMCs under flow conditions is mediated by the up-regulation of glycocalyx components, which have been previously implicated as flow shear stress sensors [35]. The inhibition of components of glycocalyx by enzymatic treatment decreases significantly the MMP13 levels, the osteogenic program of SMCs and SMCs detachment. Although the connection between MMP13 and glycocalyx has been shown previously for non-disease SMCs, we show here that the accumulation of glycocalyx is responsible for the MMP13 expression under shear stress conditions, which subsequently leads to the loss of HGPS-SMCs. It is possible that the activation of MMP13 expression triggered by an up-regulation of glycocalyx is mediated by the phosphorylation of ERK and FAK and the activation of c-Jun signaling pathway [35] or mediated via NOTCH signaling pathway [48]. Our in vivo results indicated that the expression of heparan sulfate proteoglycans in the aortic arches at week 10 on *Lmna*$^{G609G/G609G}$*Mmp13*$^{+/+}$ mice was not statistically different from the expression profile found in wild type mice. It is possible that further time is needed to see this up-regulation as seen in other progeroid animal models [3,16] or in HGPS individuals [5]. Since the upregulation of heparan sulfate was not observed in *Lmna*$^{G609G/G609G}$*Mmp13*$^{+/+}$ mice, it is not surprising that we could not observe a statistical decrease in heparan sulfate in *Lmna*$^{G609G/G609G}$*Mmp13*$^{-/-}$ mice.

The in vivo treatment results presented here using the MMP inhibitor Batimastat open possibilities for the treatment of HGPS and vascular aging [49,50]. Batimastat acts as an inhibitor of metalloproteinase activity by binding the zinc ion in the active site of MMPs. Batimastat has been used previously for the treatment of human cancer (e.g. malignant ascites [51] and malignant pleural

effusions [34]) with demonstrated results and few side-effects in phase I/II clinical trials. Therefore, the current study proposes Batimastat as a drug to be considered for future Progeria trials. It should be noted that most of the compounds identified so far in pre-clinical tests to treat Progeria have been focused: i) in the reduction of progerin quantities, by either reducing its production or increasing its degradation; ii) in the reduction of progerin toxicity by targeting its aberrant prenylation: or iii) in the identification of compounds capable of restoring pathological phenotypes downstream of progerin accumulation. Although these treatments showed encouraging results in pre-clinical studies and, in some cases in clinical trials, they do not address SMC loss over time. The administration of a drug that prevents SMC loss in early stages of disease combined with drugs that further reduce accumulation of progerin and progerin toxicity could be of added value to extend the lives of HGPS individuals.

Future studies should address the effect of SMC preservation in large vessels in the lifespan of the animals. It is possible that the prevention of SMC loss from the large arteries might be insufficient to lead to a significant increase in animal lifespan. Evidences collected at week 12 [8] (before the *Lmna*$^{G609G/G609G}$ died of progeria disease) in a therapy that ameliorated SMC loss showed no significant alterations in terms of body weight (which is correlated with lifespan [20]). Our study performed for 10 weeks showed also no significant changes in body weight (Supplementary Fig. 20d) between *Lmna*$^{G609G/G609G}$*Mmp13*$^{+/-}$ mice and *Lmna*$^{G609G/G609G}$*Mmp13*$^{+/+}$ mice. Therefore, it is possible that therapies which ameliorate SMC loss should be combined with therapies that further reduce the level of progerin in cells of the major organs, in particular the heart, which seems to present electrical defects [31]. Another issue that deserves further investigation is the relationship between MMP13 and progerin. Both in vitro and in vivo results indicate that the silencing of MMP13 leads to a significant reduction of progerin in SMCs and the reason for this pattern is presently not known. Overall, our study demonstrates that the control of MMP13 expression

decreases the vulnerability of SMCs in large vessels and this strategy may be of potential value to reduce the impact of the disease in Progeria individuals.

Methods

iPSCs culture and differentiation. iPSCs were generated from HGPS skin fibroblasts provided by Coriell Institute and characterized according to Nissan, X. *et al.* [10]. iPSCs were derived using Yamanaka's original method with OCT4, KLF4, SOX2, c-MYC, transferred using retroviral vectors. All HGPS cells were obtained from Coriell Institute for Medical Research, which in turn were collected under Institutional Review Board approval and individual informed consent (https://www.coriell.org/0/Sections/Support/NIA/Model.aspx?PgId=351). HGPS-iPSCs clone 1 (passages 43-51); HGPS-iPSCs clone 2 (passages 35-42), and N-iPSCs (passages 30-35) were maintained on mitotically inactivated mouse embryonic fibroblast (MEF) feeder layer, according to Ferreira, L.S., *et al.* [43]. Culture medium for the present work consisted of 80% KO-DMEM (Life Technologies), 0.5% L-glutamine (Life Technologies), 0.2 % β-mercaptoethanol (Sigma), 1% non-essential amino acids (Invitrogen) and penicillin-streptomycin (50 U/mL:50 mg/mL) (Lonza), supplemented with 20% KnockOut™ Serum Replacement (Gibco®) and 10 ng/mL of b-FGF (Peprotech). Colonies were expanded by routine passage every 3/4 days with 1 mg/ml collagenase type IV (Life Technologies). To induce embryoid bodies (EBs) formation, the iPSCs were treated with collagenase IV (1 mg/mL, Gibco) for 1 h and then transferred (2:1) to low attachment plates (Corning) containing 10 mL of differentiation medium (80% KO-DMEM (Life Technologies), 20% fetal bovine serum (FBS, Invitrogen), 0.5% L-glutamine (Life Technologies), 0.2% β-mercaptoethanol (Sigma), 1% non-essential amino acids (Invitrogen) and penicillin-streptomycin (50 U/mL:50 mg/mL) (Lonza). EBs were cultured for 10 days at 37 ºC, 5 % CO_2 in a humidified atmosphere, with media changes every 2 days. $CD34^+$ cells were isolated from EBs at day 10 using MACS (Miltenyi Biotec). The percentage of $CD34^+$ cells in EBs was between 0.4 and 1.5%.

Isolated cells were grown on 24-well plates (~3×10^4 cells/cm^2) coated with 0.1% gelatin in the presence of endothelial growth medium-2 (EGM-2, Lonza) supplemented with $PDGF_{BB}$ (50 ng/mL, Prepotech). After 4 passages, the medium was replaced by Smooth Muscle Growth Medium-2 (SmGM-2) (Lonza CC-3182) (maturation medium), for additional 4 passages. hVSMCs (Lonza) were used as controls for the differentiation studies. Cell cultures were maintained at 37 ºC, 5 % CO_2 in a humidified atmosphere, with media changed every 2 days. A step-by-step protocol can be found at Protocol Exchange [52].

Cell culture under arterial flow conditions. A suspension of HGPS-iPSC SMCs (clone 1), HGPS-iPSC SMCs (clone 2), N-iPSC SMCs, hVSMCs or HGPS Fibroblasts between 5 x 10^4 and 1.3 x 10^5 cells/cm^2 was applied to the entry port of an IBIDI channel (µ-Slide I ^{0,4} Luer, or µ-Slide VI ^{0,4} Luer, IBIDI) and allowed to flow inside by capillary force. After 4 h, a confluent cell layer was formed, which was then perfused with SmGM-2 medium or fibroblasts medium (DMEM supplemented with FBS (20%, v/v, Gibco), sodium pyruvate (Sigma, 1 mM) and penicillin-streptomycin (50 U/mL:50 mg/mL)) at physiological flow rate (20 dyne/cm^2). Unless specified, all tests were performed at day 0 and day 4 on flow culture conditions. Cell number and cell clumps were determined on slides stained with DAPI (20x) and normalized by image area (0.3524 mm^2). Cell clumps areas were evaluated by Image J software.

MMP activity. MMP activity was quantified on cell extracts by a fluorometric red assay kit (Abcam). Cell extracts were obtained by incubating the cells with Triton X-100 (0.5 %, v/v, in PBS, Sigma) for approximately 15 min, the cells were centrifuge and the supernatant collected. Part of cell extract (25 µL) was added to 4-aminophenylmercuric acetate (APMA, 25 µL, 2 mM) and incubated for 40 min at 37ºC. Then, a MMP red substrate (50 µL) was added to the mixture and the fluorescence intensity measured in a fluorimeter (Ex/Em=540/590 nm) after 1 h, at room

temperature. An ELISA kit was used to quantify the expression of MMP13 protein. Cell culture media collected from different experiments and plasma from WtWt and KiWt mice were used for MMP13 quantification (MMP13 human ELISA kit from Abcam and Mmp13 mouse ELISA kit from USCN) according to manufacture recommendation. Briefly, standard or sample (100 µL) were added to each well and incubate for 1 h at 37°C. Then, solutions were aspirated and detection reagent A (100 µL) was added and incubated for 1 h at 37°C. After washing 3 times, detection reagent B (100 µL) was added, incubated 30 min at 37°C and washed 5 times. Substrate solution (90 µL) was then added and left to incubate for 10-20 min at 37°C. Finally, stop solution was added to the wells (50 µL) and the absorbance of the solution monitored at 450 nm.

Glycocalyx analyses. To quantify the intensity of heparan sulfate, cells were stained with heparan sulfate (1:50 for staining, 10E4 Epitope, USBiological) as described in supplementary information. ImageJ software was used to quantify the overall intensity of each image, which was then normalized for cell number. Heparinase III from Flavobacterium heparinum (Sigma), was used for the enzymatical degradation of heparan sulfate. Briefly, HGPS-iPSC-SMCs cultured under flow condition during 4 days were subjected to heparinase III treatment (0.5 U/ml for 30 min at 37 ºC), and the number of cells per microfluidic area during culture was calculated.

Treatment of *Lmna*$^{G609G/G609G}$ mice with Batimastat. 16 *Lmna*$^{G609G/G609G}$ mice (male and female) were used. After sex and bodyweight randomization, animals were allocated in different groups and treated with vehicle (8 *Lmna*$^{G609G/G609G}$ control mice) or BB-94 inhibitor (8 *Lmna*$^{G609G/G609G}$ mice treated with Batimastat in vehicle solution). IP injections were used to administrate 30 mg/Kg/day of BB-94 at 3 mg/mL in PBS containing 0.01 % Tween 80. The treatment was administered 5 times per week during 6 weeks (from week 5 to week 10). The treatment duration was reduced from 10 to

6 weeks due to intra-abdominal accumulation of BB-94 (precipitate). At the end of week 10 the mice were sacrificed and the selected parameters were evaluated.

Double mutant generation and heart rate monitoring. *Lmna*$^{G609G/G609G}$ mice present infertility as described by Osorio and colleagues, therefore the *Lmna*$^{G609G/G609G}$ *Mmp13*$^{-/-}$ mice (KiKO) mouse were generated from *Lmna*$^{G609G/+}$ and *Mmp13*$^{-/+}$ heterozygous (in a C57BL/6 background) as our colony founders (F0). The offspring presenting the *Lmna*$^{G609G/+}$ *Mmp13*$^{-/+}$ (F1) were used for further backcrossing to generate the Progeria double mutants (KiKO) and Progeria control (KiWT) genotypes used in the present study. All mice were bred in-house in ventilated cages in a temperature and humidity-controlled room with a 12-hour light/dark cycle. The founder *Lmna*$^{G609G/+}$ mice were a kind gift from Dr. Lopez-Otin [20].

Genotyping analyses were performed to select those mice carrying the *Lmna*^{G609G} mutation in homozygosis and the MMP13 deficiency or wild type genes. Briefly, DNA was obtained from tails using the PureLink® Genomic DNA Mini Kit (Invitrogen) and DNA yields used for the PCR reaction using the Platinum®Taq DNA Polymerase (Invitrogen) and a combination of custom-designed oligonucleotides for the amplification of the *Lmna* and *Mmp13* genes. PCR products were run in agarose gels with RedSafe Nucleic Acid Staining Solution (Labotaq) for detecting the amplified Lmna DNA fragments (G609G allele at 240bp and WT at 100bp) and Mmp13 fragments (KO at 1485bp and WT at 1300 bp).

For heart rate monitoring mice were anesthetized with isoflurane (5 % induction and 2 % maintenance in oxygen) and a mouse paw pulse sensor (Kent Scientific Corporation) placed in the hindlimb paws until stable heart beats were detected and recorded by the PhysioSuiteTM non-invasive monitoring system (Kent Scientific Corporation). During the procedure and until mice recovered from anesthesia body temperature was controlled with a heating pad.

All procedures were approved by the Ethics Committee of Animal Experimentation (CCEA 57/16) of the Vall d'Hebron Research Institute and were conducted in compliance with Spanish legislation and in accordance with the Directives of the European Union.

Proteomic analysis of aortic arches from wild type and mutant mice. Formalin-fixed and paraffin embedded slices of aortic arch (4 um) were processed for mass spectrometry analysis as described in the supplementary material information and according to Heinze, I. *et al.* [33]. The obtained peptides were analyzed using Data Independent Acquisition[53] on an Orbitrap Fusion Lumos mass spectrometer (Thermo Fisher) connected online with a Waters nanoAcquity UPLC system (details regarding instrument settings and data acquisition parameters can be found in the Supplementary information). Spectral library generation, data processing and differential expression analysis was performed in Spectronaut 11 (Biognosys AG) using default settings. PCA analysis based on the protein report table exported from Spectronaut was performed using R version 3.5.0. Data are available via ProteomeXchange with identifier PXD011652 (http://proteomecentral.proteomexchange.org/cgi/GetDataset?ID=PXD011652).

Statistical analysis. Statistical analyses were performed with GraphPad Prism software. Statistical significance was analyzed using two-tailed unpaired Student's t test between two different groups. For multiple comparisons, a one-way ANOVA analysis followed by Newman-Keuls post-test was performed. Results were considered significant when $p < 0.05$. Data are shown as mean ± SEM unless other specification.

Data availability

The microarray datasets generated during and/or analyzed during the current study are available in the GEO/NCBI (GEO accession: GSE108368, https://www.ncbi.nlm.nih.gov/geo/query/acc.cgi?acc=GSE108368).

The mass spectrometry proteomics data that support the findings of this study have been deposited in the ProteomeXchange Consortium via the PRIDE[54] partner repository with the dataset identifier PXD011652 (http://proteomecentral.proteomexchange.org/cgi/GetDataset?ID=PXD011652).

The mass spectrometry proteomics (Tandem Mass Tags - TMT) data have been deposited to the ProteomeXchange Consortium via the PRIDE[54] partner repository with the dataset identifier PXD019316 (http://proteomecentral.proteomexchange.org/cgi/GetDataset?ID=PXD019316).

Databases used: Uniprot database (Swissprot entry only, release 2016_01, 16,747 entries); CellAge database (http://genomics.senescence.info/cells/).

The authors declare that the data supporting the findings of this study are available within the paper and its supplementary information files. All the figures have associated source data.

No restriction is applied to the data presented.

References:

1. Hennekam, R.C. Hutchinson-Gilford progeria syndrome: review of the phenotype. *Am J Med Genet A* **140**, 2603-2624 (2006).
2. Eriksson, M.*, et al.* Recurrent de novo point mutations in lamin A cause Hutchinson-Gilford progeria syndrome. *Nature* **423**, 293-298 (2003).
3. Varga, R.*, et al.* Progressive vascular smooth muscle cell defects in a mouse model of Hutchinson-Gilford progeria syndrome. *Proceedings of the National Academy of Sciences of the United States of America* **103**, 3250-3255 (2006).
4. Hamczyk, M.R.*, et al.* Vascular Smooth Muscle-Specific Progerin Expression Accelerates Atherosclerosis and Death in a Mouse Model of Hutchinson-Gilford Progeria Syndrome. *Circulation* **138**, 266-282 (2018).
5. Olive, M.*, et al.* Cardiovascular pathology in Hutchinson-Gilford progeria: correlation with the vascular pathology of aging. *Arterioscler Thromb Vasc Biol* **30**, 2301-2309 (2010).
6. Liu, Y., Drozdov, I., Shroff, R., Beltran, L.E. & Shanahan, C.M. Prelamin A accelerates vascular calcification via activation of the DNA damage response and senescence-associated secretory phenotype in vascular smooth muscle cells. *Circ Res* **112**, e99-109 (2013).
7. Zhang, H., Xiong, Z.M. & Cao, K. Mechanisms controlling the smooth muscle cell death in progeria via down-regulation of poly(ADP-ribose) polymerase 1. *Proceedings of the National Academy of Sciences of the United States of America* **111**, E2261-2270 (2014).
8. Kim, P.H.*, et al.* Disrupting the LINC complex in smooth muscle cells reduces aortic disease in a mouse model of Hutchinson-Gilford progeria syndrome. *Sci Transl Med* **10**(2018).
9. Liu, G.H.*, et al.* Recapitulation of premature ageing with iPSCs from Hutchinson-Gilford progeria syndrome. *Nature* **472**, 221-225 (2011).
10. Nissan, X.*, et al.* Unique preservation of neural cells in Hutchinson- Gilford progeria syndrome is due to the expression of the neural-specific miR-9 microRNA. *Cell Rep* **2**, 1-9 (2012).
11. Chen, Z.*, et al.* Reprogramming progeria fibroblasts re-establishes a normal epigenetic landscape. *Aging cell* **16**, 870-887 (2017).
12. Frid, M.G., Shekhonin, B.V., Koteliansky, V.E. & Glukhova, M.A. Phenotypic changes of human smooth muscle cells during development: late expression of heavy caldesmon and calponin. *Dev Biol* **153**, 185-193 (1992).
13. Duband, J.L., Gimona, M., Scatena, M., Sartore, S. & Small, J.V. Calponin and SM 22 as differentiation markers of smooth muscle: spatiotemporal distribution during avian embryonic development. *Differentiation* **55**, 1-11 (1993).
14. Vazao, H., das Neves, R.P., Graos, M. & Ferreira, L. Towards the maturation and characterization of smooth muscle cells derived from human embryonic stem cells. *PLoS One* **6**, e17771 (2011).
15. Scaffidi, P. & Misteli, T. Lamin A-dependent misregulation of adult stem cells associated with accelerated ageing. *Nat Cell Biol* **10**, 452-459 (2008).
16. Capell, B.C.*, et al.* Inhibiting farnesylation of progerin prevents the characteristic nuclear blebbing of Hutchinson-Gilford progeria syndrome. *Proceedings of the National Academy of Sciences of the United States of America* **102**, 12879-12884 (2005).
17. Toth, J.I.*, et al.* Blocking protein farnesyltransferase improves nuclear shape in fibroblasts from humans with progeroid syndromes. *Proc Natl Acad Sci U S A* **102**, 12873-12878 (2005).
18. Mallampalli, M.P., Huyer, G., Bendale, P., Gelb, M.H. & Michaelis, S. Inhibiting farnesylation reverses the nuclear morphology defect in a HeLa cell model for Hutchinson-Gilford progeria syndrome. *Proc Natl Acad Sci U S A* **102**, 14416-14421 (2005).
19. Chiu, J.J. & Chien, S. Effects of disturbed flow on vascular endothelium: pathophysiological basis and clinical perspectives. *Physiol Rev* **91**, 327-387 (2011).
20. Osorio, F.G.*, et al.* Splicing-directed therapy in a new mouse model of human accelerated aging. *Sci Transl Med* **3**, 106ra107 (2011).
21. Santiago-Fernandez, O.*, et al.* Development of a CRISPR/Cas9-based therapy for Hutchinson-Gilford progeria syndrome. *Nat Med* **25**, 423-426 (2019).

22. Shimizu, T.*, et al.* Notch signaling induces osteogenic differentiation and mineralization of vascular smooth muscle cells: role of Msx2 gene induction via Notch-RBP-Jk signaling. *Arterioscler Thromb Vasc Biol* **29**, 1104-1111 (2009).
23. Cheng, C.*, et al.* Large variations in absolute wall shear stress levels within one species and between species. *Atherosclerosis* **195**, 225-235 (2007).
24. Suo, J.*, et al.* Hemodynamic shear stresses in mouse aortas: implications for atherogenesis. *Arterioscler Thromb Vasc Biol* **27**, 346-351 (2007).
25. Tacutu, R.*, et al.* Human Ageing Genomic Resources: integrated databases and tools for the biology and genetics of ageing. *Nucleic Acids Res* **41**, D1027-1033 (2013).
26. Knauper, V.*, et al.* Cellular mechanisms for human procollagenase-3 (MMP-13) activation. Evidence that MT1-MMP (MMP-14) and gelatinase a (MMP-2) are able to generate active enzyme. *J Biol Chem* **271**, 17124-17131 (1996).
27. Wojtowicz-Praga, S.*, et al.* Phase I trial of a novel matrix metalloproteinase inhibitor batimastat (BB-94) in patients with advanced cancer. *Invest New Drugs* **14**, 193-202 (1996).
28. Quillard, T.*, et al.* Selective inhibition of matrix metalloproteinase-13 increases collagen content of established mouse atherosclerosis. *Arterioscler Thromb Vasc Biol* **31**, 2464-2472 (2011).
29. Engel, C.K.*, et al.* Structural basis for the highly selective inhibition of MMP-13. *Chem Biol* **12**, 181-189 (2005).
30. Villa-Bellosta, R.*, et al.* Defective extracellular pyrophosphate metabolism promotes vascular calcification in a mouse model of Hutchinson-Gilford progeria syndrome that is ameliorated on pyrophosphate treatment. *Circulation* **127**, 2442-2451 (2013).
31. Rivera-Torres, J.*, et al.* Cardiac electrical defects in progeroid mice and Hutchinson-Gilford progeria syndrome patients with nuclear lamina alterations. *Proceedings of the National Academy of Sciences of the United States of America* **113**, E7250-E7259 (2016).
32. Buczak, K.*, et al.* Spatial Tissue Proteomics Quantifies Inter- and Intratumor Heterogeneity in Hepatocellular Carcinoma (HCC). *Mol Cell Proteomics* **17**, 810-825 (2018).
33. Heinze, I.*, et al.* Species comparison of liver proteomes reveals links to naked mole-rat longevity and human aging. *BMC Biol* **16**, 82 (2018).
34. Macaulay, V.M.*, et al.* Phase I study of intrapleural batimastat (BB-94), a matrix metalloproteinase inhibitor, in the treatment of malignant pleural effusions. *Clin Cancer Res* **5**, 513-520 (1999).
35. Shi, Z.D., Wang, H. & Tarbell, J.M. Heparan sulfate proteoglycans mediate interstitial flow mechanotransduction regulating MMP-13 expression and cell motility via FAK-ERK in 3D collagen. *PLoS One* **6**, e15956 (2011).
36. Ainslie, K.M., Garanich, J.S., Dull, R.O. & Tarbell, J.M. Vascular smooth muscle cell glycocalyx influences shear stress-mediated contractile response. *J Appl Physiol (1985)* **98**, 242-249 (2005).
37. Knauper, V.*, et al.* The role of the C-terminal domain of human collagenase-3 (MMP-13) in the activation of procollagenase-3, substrate specificity, and tissue inhibitor of metalloproteinase interaction. *J Biol Chem* **272**, 7608-7616 (1997).
38. Austin, K.M., Covic, L. & Kuliopulos, A. Matrix metalloproteases and PAR1 activation. *Blood* **121**, 431-439 (2013).
39. Gordon, L.B.*, et al.* Clinical trial of a farnesyltransferase inhibitor in children with Hutchinson-Gilford progeria syndrome. *Proc Natl Acad Sci U S A* **109**, 16666-16671 (2012).
40. Varela, I.*, et al.* Combined treatment with statins and aminobisphosphonates extends longevity in a mouse model of human premature aging. *Nat Med* **14**, 767-772 (2008).
41. Song, M., San, H., Anderson, S.A., Cannon, R.O., 3rd & Orlic, D. Shear stress-induced mechanotransduction protein deregulation and vasculopathy in a mouse model of progeria. *Stem Cell Res Ther* **5**, 41 (2014).
42. Cheung, C., Bernardo, A.S., Pedersen, R.A. & Sinha, S. Directed differentiation of embryonic origin-specific vascular smooth muscle subtypes from human pluripotent stem cells. *Nat Protoc* **9**, 929-938 (2014).
43. Ferreira, L.S.*, et al.* Vascular progenitor cells isolated from human embryonic stem cells give rise to endothelial and smooth muscle like cells and form vascular networks in vivo. *Circ Res* **101**, 286-294 (2007).
44. Maguire, E.M., Xiao, Q. & Xu, Q. Differentiation and Application of Induced Pluripotent Stem Cell-Derived Vascular Smooth Muscle Cells. *Arterioscler Thromb Vasc Biol* **37**, 2026-2037 (2017).

45. Zhang, J., *et al.* A human iPSC model of Hutchinson Gilford Progeria reveals vascular smooth muscle and mesenchymal stem cell defects. *Cell Stem Cell* **8**, 31-45 (2011).
46. Inada, M., *et al.* Critical roles for collagenase-3 (Mmp13) in development of growth plate cartilage and in endochondral ossification. *Proc Natl Acad Sci U S A* **101**, 17192-17197 (2004).
47. Capell, B.C., *et al.* A farnesyltransferase inhibitor prevents both the onset and late progression of cardiovascular disease in a progeria mouse model. *Proc Natl Acad Sci U S A* **105**, 15902-15907 (2008).
48. Xiao, D., *et al.* Notch Signaling Regulates MMP-13 Expression via Runx2 in Chondrocytes. *Sci Rep* **9**, 15596 (2019).
49. Cathcart, J.M. & Cao, J. MMP Inhibitors: Past, present and future. *Front Biosci (Landmark Ed)* **20**, 1164-1178 (2015).
50. Nosoudi, N., *et al.* Prevention of abdominal aortic aneurysm progression by targeted inhibition of matrix metalloproteinase activity with batimastat-loaded nanoparticles. *Circ Res* **117**, e80-89 (2015).
51. Parsons, S.L., Watson, S.A. & Steele, R.J. Phase I/II trial of batimastat, a matrix metalloproteinase inhibitor, in patients with malignant ascites. *Eur J Surg Oncol* **23**, 526-531 (1997).
52. Pitrez, P.R., *et al.* Differentiation of human induced-pluripotent stem cells into smooth muscle cells. *Protoc. Exch.* https://doi.org/10.1038/10.21203/rs.3.pex-964/v1 (2020).
53. Bruderer, R., *et al.* Extending the limits of quantitative proteome profiling with data-independent acquisition and application to acetaminophen-treated three-dimensional liver microtissues. *Mol Cell Proteomics* **14**, 1400-1410 (2015).
54. Vizcaino, J.A., *et al.* 2016 update of the PRIDE database and its related tools. *Nucleic Acids Res* **44**, 11033 (2016).

Acknowledgments

This work was funded by FEDER through the Program COMPETE and by Portuguese fund through FCT in context of the projects EXPL/BIM-MED/2267/2013 and POCI-01-0145-FEDER-029229, as well as the European project ERAatUC (ref. 669088). PRP wishes to thank FCT for a BD fellowship (SFRH/BD/71042/2010). AR is supported by the Miguel Servet research contract CPII15/00003 from Instituto de Salud Carlos III, Spain. The FLI is a member of the Leibniz Association and is financially supported by the Federal Government of Germany and the State of Thuringia. The authors gratefully acknowledge support from the FLI proteomics core facility. The authors would like to thank Dr. Carlos Lopez-Otín for providing the *Lmna*$^{G609G/+}$ mice. The authors have no conflict of interest to disclose. All data is available in the main text or the supplementary materials.

Author contributions

PRP and LF designed the study, did the literature search and wrote the manuscript. PRP conducted the study. PRP, LE and HV collected the *in vitro* data. PRP, GC, AR, ASG, KH, CN, NL conducted and analyzed in vivo data. DT and JPM processed and analyzed raw genomic data. ALE and XN generated iPSCs from Progeria fibroblasts, provided expertise in the Progeria biology and in the interpretation of the results. LM, AB, RS, PRP, LF and JS generated the isogenic cell line. TC performed pathological evaluation of the tissues. DS performed proteomics experiments and analyzed the data with the support of AO.

Competing Interests

The authors declare no competing interests.

Supplementary Information accompanies this paper.

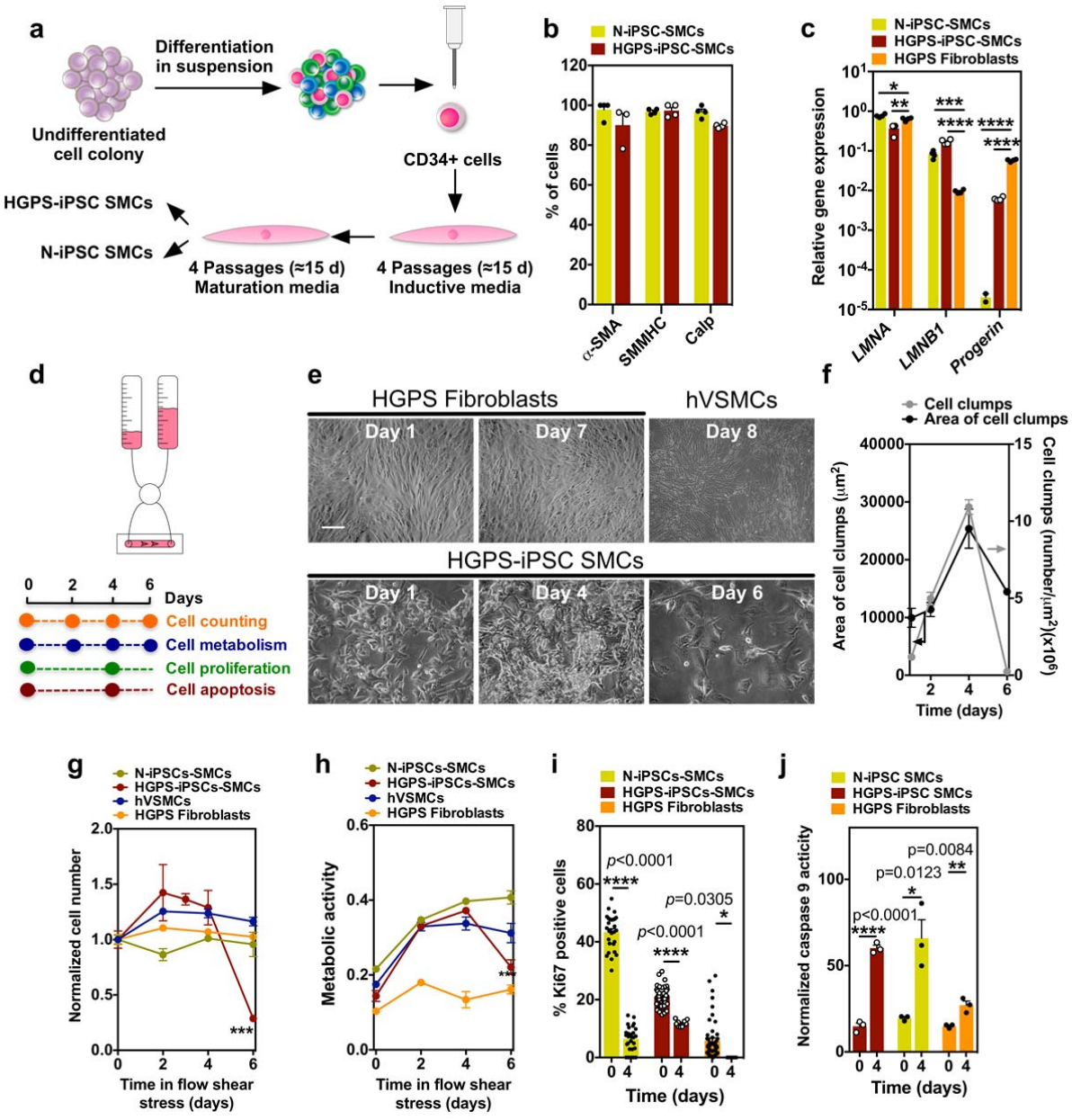

Fig. 1: Vulnerability of HGPS-iPSC SMCs to arterial flow conditions. a Schematic representation of the methodology used to differentiate iPSCs into SMCs. **b** Expression of SMC markers on iPSC-derived SMCs. Percentage of positive cells expressing SMC markers as evaluated by immunofluorescence (at least 100 cells were counted per each marker). Results are Mean ± SEM (n=3 independent experiments). **c** Expression of progeria markers on iPSC-derived SMCs. Gene expression by qRT-PCR (gene expression was normalized by the housekeeping gene *GAPDH*).

753 HGPS Fibroblasts were used as control. Results are Mean ± SEM (n=4 technical replicates from a
754 pool of 3 independent experiments). *,**,***,**** denotes statistical significance (p<0.05, p<0.01,
755 p<0.001, p<0.0001). Statistical analyses were performed by one-way ANOVA followed by
756 Newman Keuls's post-test. **d** Schematic representation of the protocol used. Cells were cultured for
757 6-8 days in arterial flow conditions (20 dyne/cm^2). **e** Light microscopy images of HGPS
758 Fibroblasts, hVSMCs or HGPS-iPSC SMCs (10% of the cells accumulate progerin protein) at
759 different culture days. Only HGPS-iPSC SMCs detached from the microfluidic system at day 4.
760 Scale bar is 50 μm. **f** Number and area of cell clumps in HGPS-iPSC SMCs at different times (at
761 least 2 images (×10) have been quantified per time). For area of cell clumps n>2 images examined
762 over 3 independent experiments; for cell clumps, n=3 independent experiments. **g** Number of cells
763 per surface area (mm^2) during cell culture under arterial flow (at least 3 images (×10) have been
764 quantified per time; n=3-7 independent experiments). Cell number was normalized by the number
765 of cells present at day 0. **h** Cell metabolism evaluated by Presto Blue assay. Absorbance at 570 nm
766 was measured and normalized to the 600 nm values for the experimental wells. n=3 independent
767 experiments. **i** Expression of nuclear proliferation marker, Ki67 (at least 3 images (×10) have been
768 quantified per time). The percentage of Ki67 positive cells was evaluated by immunofluorescence.
769 n>3 images examined over 3 independent experiments. **j** Cell apoptosis evaluated by caspase-9
770 activity. Results were normalized by cell number. n=3 independent experiments. From c to g,
771 results are Mean ± SEM. *,**,***,**** denotes statistical significance (p<0.05, p<0.01, p<0.001,
772 p<0.0001). Statistical analyses were performed by a two-tailed unpaired Student's t-test **i** and **j**.
773

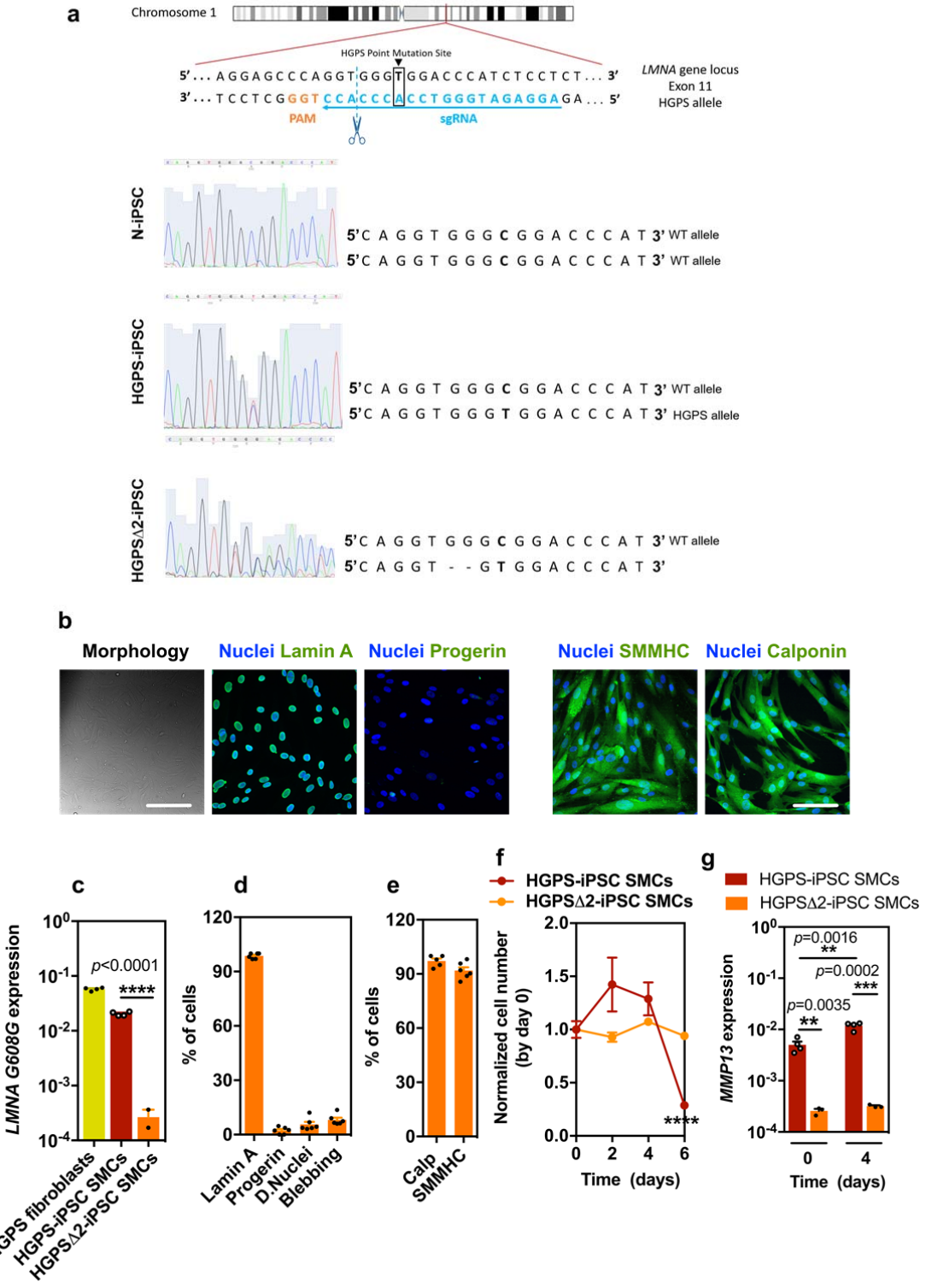

774

775 **Fig. 2: Expression of progeria and SMC markers in HGPSΔ2-iPSC SMCs. a** gRNA directs

776 Cas9 nuclease against mutated exon 11 of *LMNA* gene, upstream the HGPS mutation, disrupting

progerin, without altering lamin A and lamin C. Sanger sequencing for *LMNA* (NM_170707.4 transcript) exon 11 was performed for: N-iPSCs, HGPS-iPSCs and HGPSΔ2-iPSCs, confirming the deletion of 2 base pairs in the HGPSΔ2-iPSCs. **b** Expression of lamin A, progerin and SMC proteins monitored by immunofluorescence. Scale bar is 100 μm. n=6 independent experiments. **c** Expression of *progerin (LMNA G608G* gene) in HGPS and HGPSΔ2 cell lines. Results are Mean ± SEM (n=4 technical replicates from a pool of 3 independent experiments). Statistical analyses were performed by a two-tailed unpaired Student's t-test. **d** Quantification of lamin A, progerin, dysmorphic nuclei and nuclei blebbing. Results are Mean ± SEM (n=6 independent experiments). **** denotes statistical significance (p<0.0001). **e** Percentage of cells that have been differentiated from HGPSΔ2-iPSCs that express SMC markers at protein level. Results are Mean ± SEM (n=5-6 independent experiments). **f** Number of cells per surface (mm^2) as quantified by high-content microscopy (at least 3 images (×10) have been quantified per time). The number of cells was evaluated after 6 days under arterial flow and was normalized by the number of cells present at day 0. n>3 images examined over 3 independent experiments. **g** *MMP13* mRNA transcripts quantified by qRT-PCR analyses in HGPS-iPSC SMCs or HGPSΔ2-iPSC SMCs cultured under flow conditions. MMP13 mRNA transcripts were normalized by *GAPDH*. n=4 technical replicates from a pool of 3 independent experiments. **,*** denotes statistical significance (p<0.01, p<0.001). Statistical analyses were performed by a two-tailed unpaired Student's t-test.

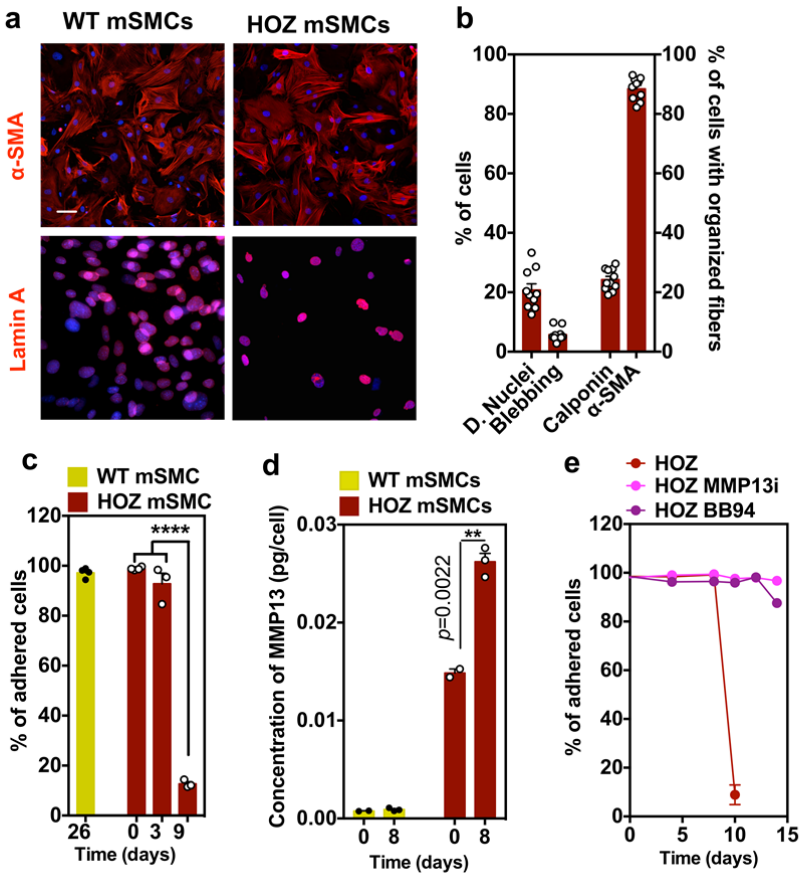

Fig. 3: Characterization and impact of flow shear stress in SMCs isolated from wild type (WT) and homozygous (HOZ) *Lmna*$^{G609G/G609G}$ mice. a Mouse SMCs were cultured for 9-26 days in arterial flow conditions (120 dyne/cm^2). Immunofluorescence analyses performed on mouse SMCs (6-week-old wild-type and homozygous *Lmna* $^{G609G/G609G}$ mice) at passage 4 for α-SMA and Lamin A. Nuclei was stained with DAPI. Scale bar is 20 µm. n=3-4 images examined over 3 independent experiments. **b** Percentage of dysmorphic nuclei, nuclei blebbing and SMC organized fibers in mSMCs (assessed in static conditions). n=3-4 images examined over 3 independent experiments. **c** Percentage of adhered cells over time. Cells were cultured under flow conditions. n=3-4 independent experiments. Statistical analyses were performed by one-way ANOVA followed by Newman Keuls's post-test. **d** Quantification of MMP13 in HOZ mSMCs and WT mSMCs. Cells were analyzed at day 0 and day 8 under flow. Fluorescence signal was normalized by cell number. n=3-4 independent experiments. Statistical analyses were performed by a two-tailed

unpaired Student's t-test. **e** Percentage of adhered cells over time. Cells were cultured under flow conditions. n=5-6 independent experiments. In graphs b-e, results are Mean ± SEM. *,**,***,**** denotes statistical significance ($p<0.05$, $p<0.01$, $p<0.001$, $p<0.0001$).

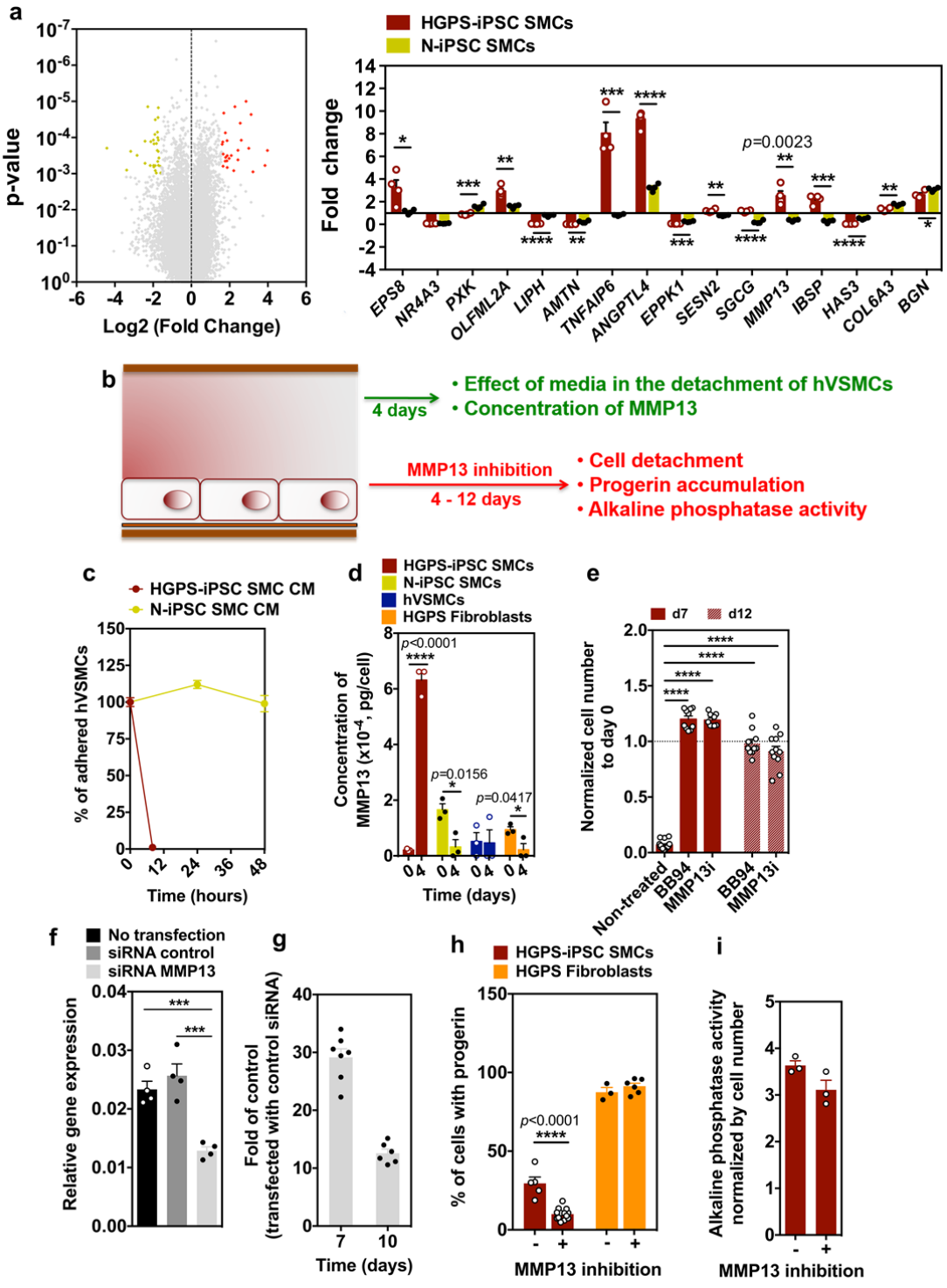

Fig. 4: MMP13 activity in HGPS-iPSC SMCs cultured under flow shear stress. a Volcano plot representing differentially expressed genes in HGPS-iPSC-SMC cultured under flow conditions at day 0 and 4. Each point represents one of 53617 genes. 26 and 31 genes were upregulated (red; fold

820 change >= 3; p<0.001) and downregulated (yellow; fold change <= 3; p<0.001), respectively.
821 Graph shows qRT-PCR validation for 16 genes with fold-changes greater than 3. Fold change was
822 between day 0 and day 4. Gene expression was normalized by the housekeeping gene *GAPDH*.
823 Results are Mean ± SEM, n=4 technical replicates from a pool of 3 independent experiments.
824 Statistical analyses were performed by a two-tailed unpaired Student's t-test. **b** Schematic
825 representation of the experimental protocol used. **c** Effect of HGPS-iPSC SMC or N-iPSC SMCs
826 conditioned media (in both cases obtained after 4 days under flow conditions) on hVSMCs cultured
827 under flow conditions. n=1-5 images examined over 3 independent experiments. **d** Quantification of
828 MMP13 activity (cell culture media) by ELISA. Cells were analyzed at day 0 and day 4 under flow.
829 Fluorescence signal was normalized by cell number. n=3 independent experiments. Statistical
830 analyses were performed by a two-tailed unpaired Student's t-test. **e** Effect of MMP13 or BB94
831 inhibition in HGPS-iPSC SMC detachment. The number of cells was evaluated after 7 and 12 days
832 under arterial flow and was normalized by the number of cells present at day 0. n=3-5 images
833 examined over 3 independent experiments. Statistical analyses were performed by one-way
834 ANOVA followed by Newman Keuls's post-test. **f** MMP13 knock down by siRNA in HGPS-iPSC
835 SMCs. *MMP13* mRNA transcripts were quantified by qRT-PCR and normalized by *GAPDH*. Mean
836 ± SEM (n=4 technical replicates from a pool of 3 independent experiments). Statistical analyses
837 were performed by one-way ANOVA followed by Newman Keuls's post-test. **g** Number of cells
838 per microfluidic area during culture under flow shear conditions normalized by the number of cells
839 in control experimental groups (i.e., cells transfected with control siRNA). n=7 independent
840 experiments for day 7 and n=6 independent experiments for day 10. **h** Percentage of progerin
841 positive cells after 7 days under flow conditions with SmGM2 media supplemented or not with
842 MMP13 inhibitor. n=1 to 5 images examined over 3 independent experiments. Statistical analyses
843 were performed by a two-tailed unpaired Student's t-test. **i** Activity of alkaline phosphatase in
844 HGPS-iPSCs-SMC normalized by cell number per mm^2, in cells cultured 4 days under flow

conditions. Cells were treated or not with MMP13 inhibitor. n=3 independent experiments. In graphs a-h, results are Mean ± SEM. *,**,***,**** denotes statistical significance ($p<0.05$, $p<0.01$, $p<0.001$, $p<0.0001$).

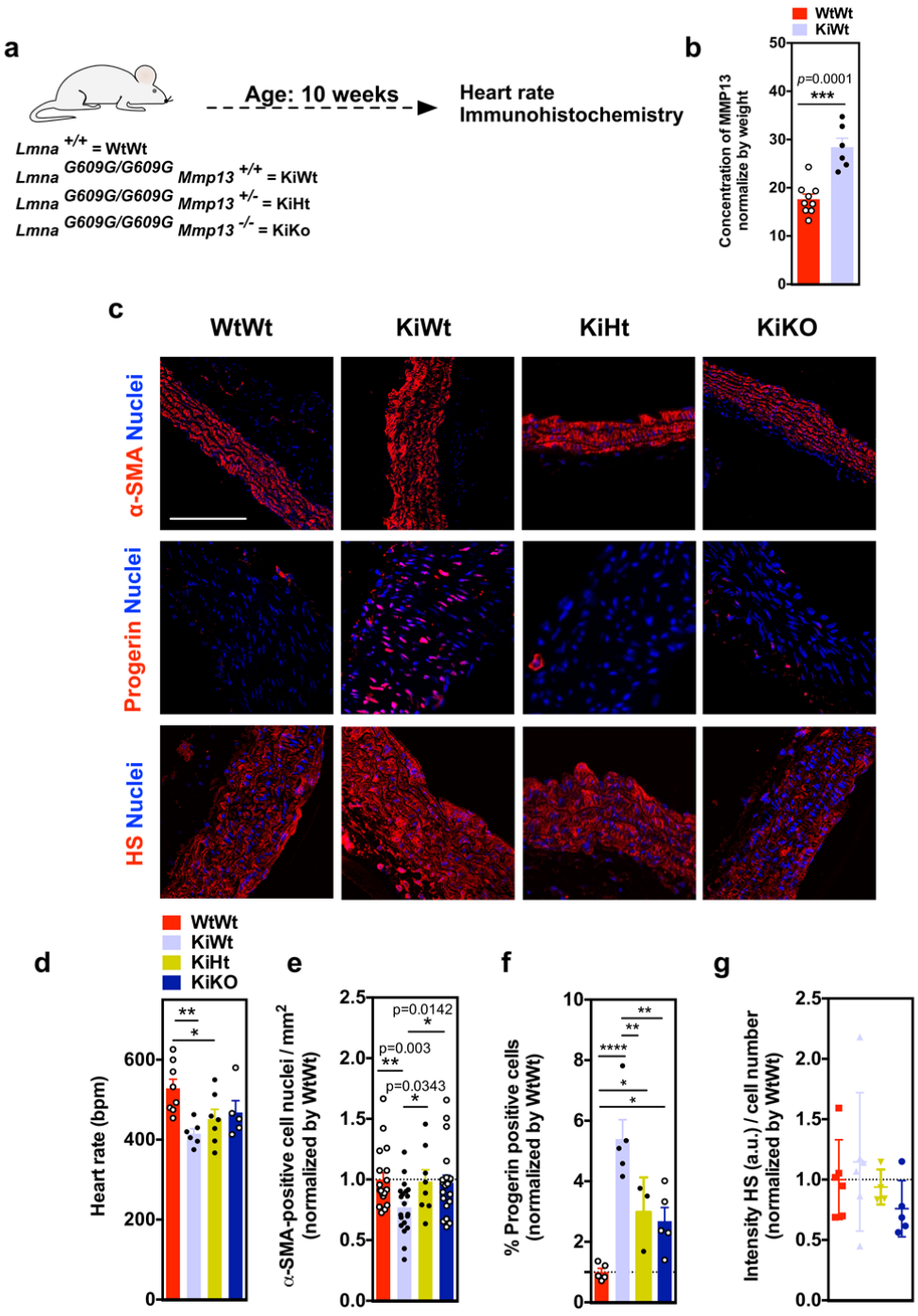

Fig. 5: MMP13 inhibition significantly increases SMC number in aortic arch of *Lmna*$^{G609G/G609G}$ mice. a Schematic representation of the animal protocol. WtWt, KiWt, KiHt and KiKo mice (age: 10 weeks) were evaluated. **b** Quantification of MMP13 activity (plasma from WtWt, n=9, and KiWt, n=6, mice) by ELISA. Fluorescence signal was normalized by mice weight. Statistical analyses were performed by a two-tailed unpaired Student's t-test. **c** Immunofluorescence

857 analyses in the aortic arch for α-SMA, progerin and heparan sulfate (HS). Cell nuclei were stained
858 with DAPI. Scale bar is 100 µm for α-SMA staining and 50 µm for progerin and heparan sulfate
859 staining. For α-SMA staining, n=5 animals, except for KiHt (4 animals). For progerin staining, n=5
860 animals, except for KiHt (3 animals). For heparan sulfate n=6 WtWt, n=6 KiWt, n=4 KiHt and n=5
861 for KiKo. **d** Heart rates in mice (n=8 WtWt, n=6 KiWt, n=7 KiHt and n=5 KiKo). Statistical
862 analyses were performed by one-way ANOVA followed by Newman Keuls's post-test. **e** Number
863 of SMC nuclei in aortic arch per tissue area (mm^2) (n=2-3 slides examined over 5 animals, except
864 for KiHt (4 animals). Statistical analyses were performed by a two-tailed unpaired Student's t-test.
865 **f** Percentage of progerin positive cells in SMCs. n=5 animals, except for KiHt (3 animals).
866 Statistical analyses were performed by one-way ANOVA followed by Newman Keuls's post-test. **g**
867 Expression of heparan sulfate as evaluated by immunofluorescence. Intensity of heparan sulfate was
868 calculated in each picture (at least 16 pictures per condition) and normalized by cell number mice
869 (n=6 WtWt, n=6 KiWt, n=4 KiHt and n=5 KiKo). In **b**, **d**, **e**, **f** and **g**, results are Mean ± SEM.
870 *,**,***,**** denotes statistical significance ($p<0.05$, $p<0.01$, $p<0.001$, $p<0.0001$).
871
872

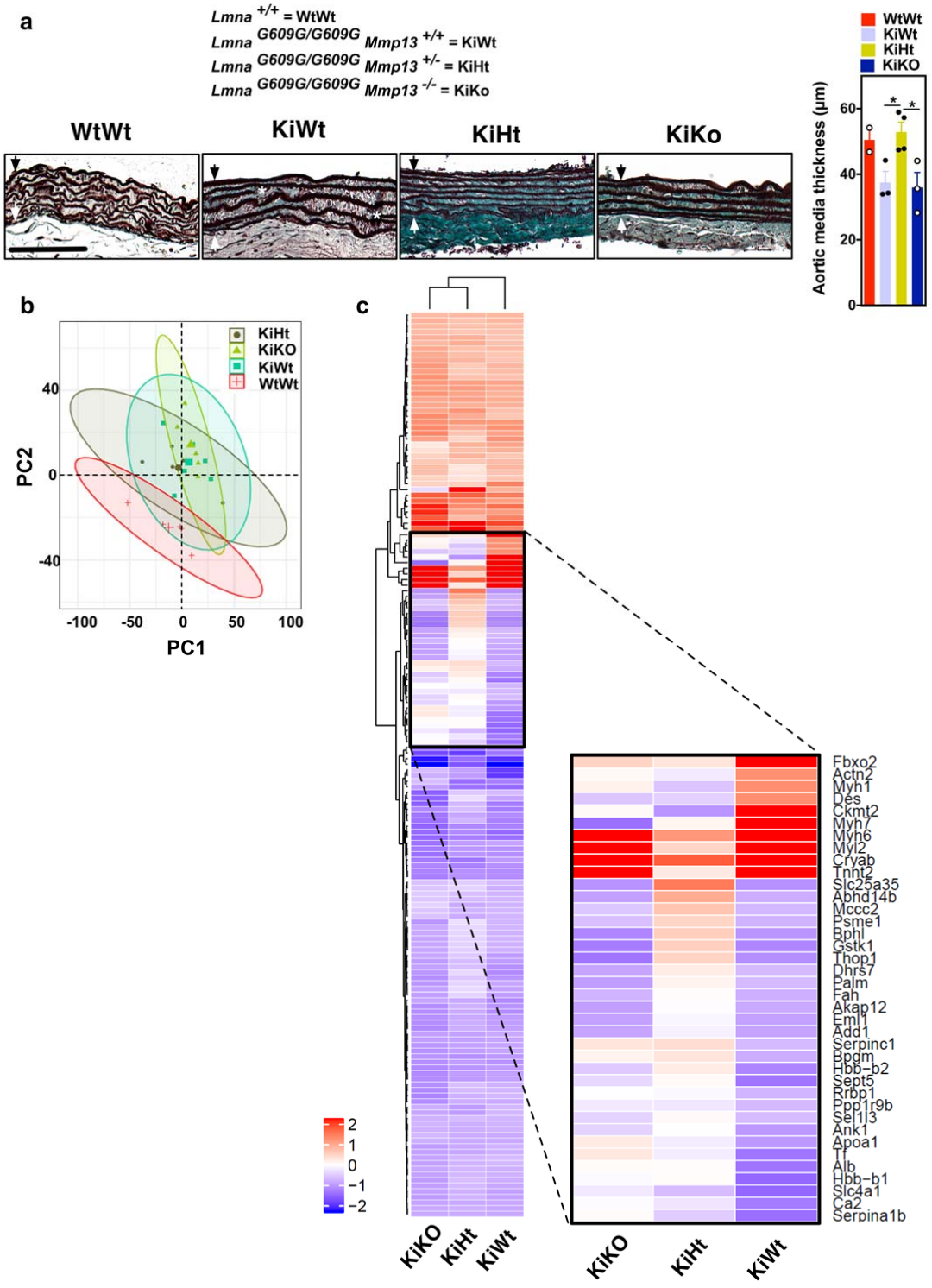

873

874 **Fig. 6: Proteins differentially expressed in the aortic arch at week 10 on wild type and mutant**

875 **(*Lmna*$^{G609G/G609G}$*Mmp13*$^{-/-}$ and *Lmna*$^{G609G/G609G}$*Mmp13*$^{+/-}$) mice. a** Orcein-stained ascending aorta

876 (elastic fibers stain in dark brown/black). Black arrow defines the internal elastic lamina while the

white arrow defines the adventitial border. Images illustrate morphological changes rather than aortic media thickness differences. KiWT mice shows less compact elastic lamellae and higher irregular profiles of the elastic lamellae (labelled with *) than the other mice. Scale bar is 50 µm. In graph, aortic media thickness was measured from the internal elastic lamina to the adventitial border. Black arrow defines the internal elastic lamina while the white arrow defines the adventitial border. Results are Mean ± SEM, n=3 animals, except for KiHt (4 animals). * denotes statistical significance ($p<0.05$). Statistical analyses were performed by one-way ANOVA followed by Newman Keuls's post-test. **b** Principal component analysis (PCA) of proteome profiles obtained from aortic arches of wild type (WtWt) and mutant (KiWt, KiHt, KiKo) mice. **c** Heatmap based on 161 protein groups differentially expressed between KiWt and WtWt mice, in aortic arch, at week 10 ($q<0.05$ and abs($\log_2$ fold change)>0.58). Progerin is a mutated protein and thus not identified by the mass spectrometry. MMP13 is a secreted protein and the levels in cells were not detectable by mass spectrometry. For comparison purposes, the protein fold changes of WtWt vs KiHt and WtWt *vs* KIKo were included in the heatmap. Blue color indicates proteins down-regulated in KiWt, KiHt or KiKo as compared to WtWt, whereas red color corresponds to proteins up-regulated in KiWt, KiHt or KiKo as compared to WtWt. n=6 for KiWt and n=5 for WtWt, KiHt and KiKo; age: 10 weeks.

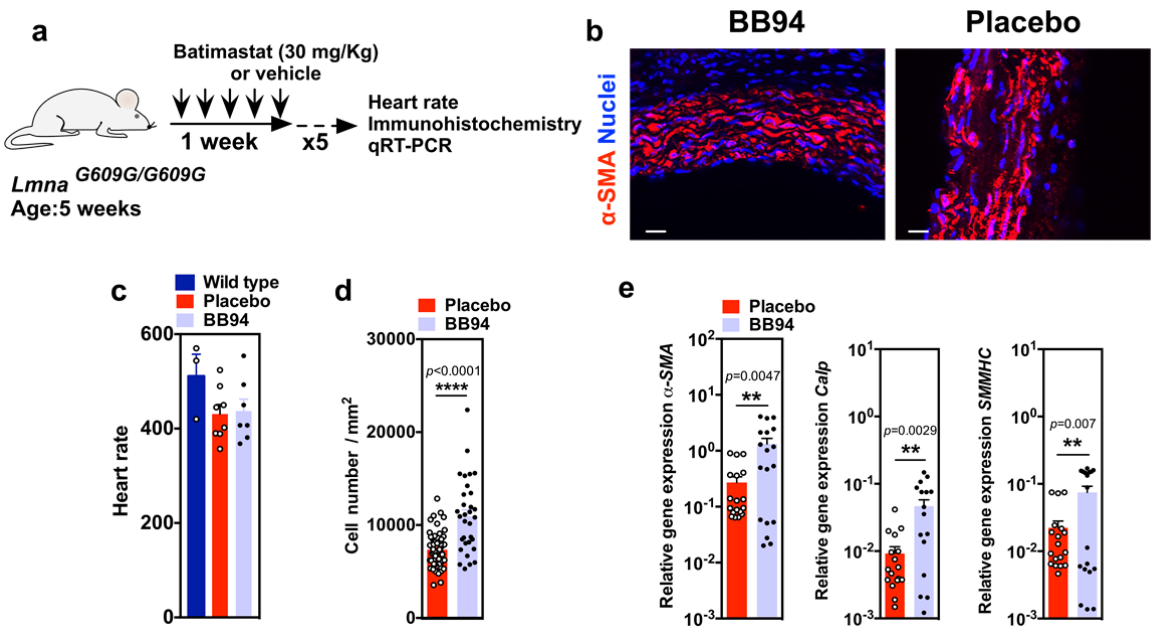

Fig. 7: MMP treatment using BB94 significantly increases SMC number in aortic arch of *Lmna*$^{G609G/G609G}$ mice. a Schematic representation of the animal protocol. *Lmna*$^{G609G/G609G}$ mice (n=8 for treatment group and control group; age: 5 weeks) were IP injected 5 times a week (30 mg/Kg/day; 3 mg/mL in PBS). **b** Immunofluorescence analyses performed on mouse SMC for α-SMA showing higher number of SMCs in treated aortic arch. Cell nuclei were stained with DAPI. SMCs were stained for α-SMA. Scale bar is 100 µm. For BB94 treatment n=5 animals. For Placebo treatment n=7 animals. **c** Heart rates in mice. Wild type mice were not exposed to BB94. n=3 for wild type mice, n=8 for Placebo treatment group and n=7 for BB94 treatment group. **d** Number of SMC nuclei in aortic arch per tissue area (mm^2) in mice treated or not with BB94. For BB94 treatment, n>6 images examined over 5 animals. For Placebo treatment, n>9 images examined over 7 animals. **e** Expression of SMC genes in aortic arches of mice treated or not with BB94. Gene expression was normalized by the housekeeping gene *GAPDH*. n>3 technical replicates over 6 animals **,***, **** denotes statistical significance (p<0.01, p<0.001, p<0.0001). Statistical analyses were performed by a two-tailed unpaired Student's t-test **d** and **e**.

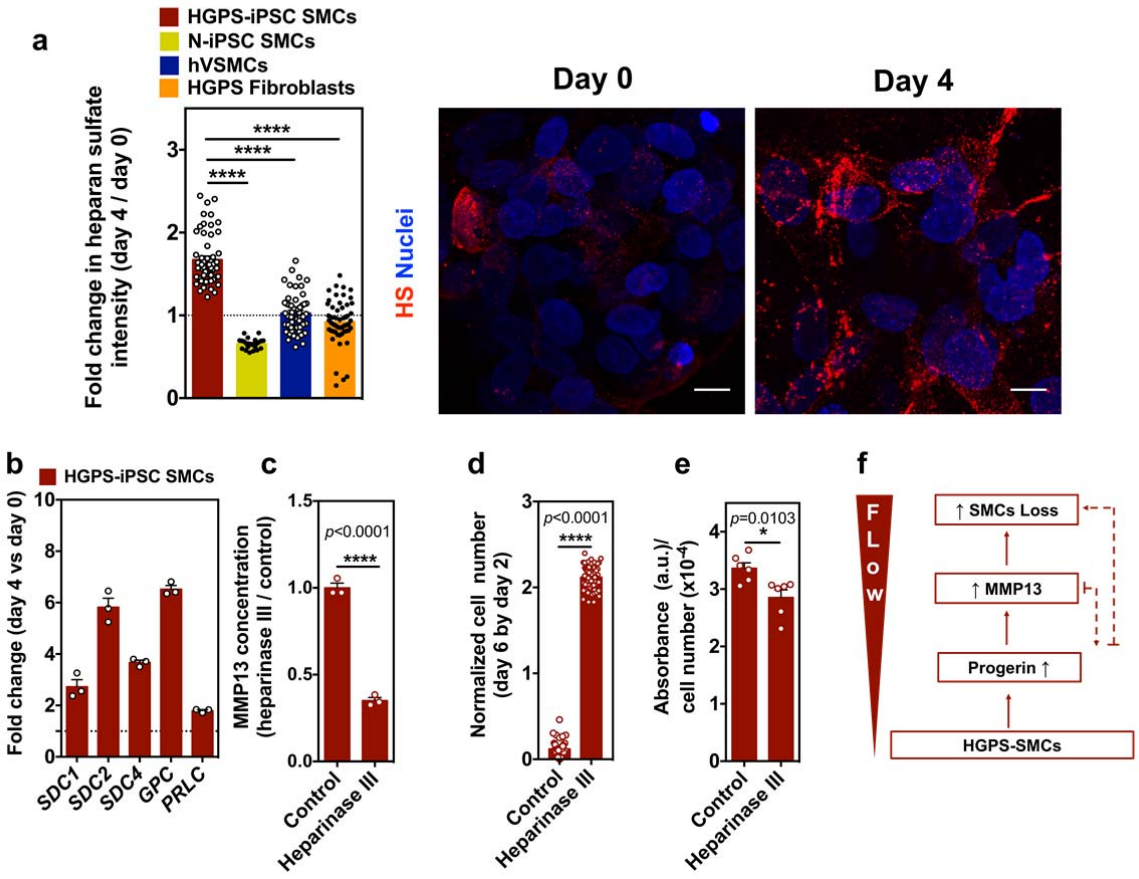

Fig. 8: MMP13 expression in SMCs is triggered by an increase in heparan sulfate. **a** Cells were cultured under flow conditions for 4 days and the expression of heparan sulfate was evaluated by immunofluorescence. Intensity of heparan sulfate was calculated in each picture and normalized by cell number. The normalized fluorescence intensity at day 4 was divided with the one at day 0. Scale bar is 10 µm. n>4 images examined over 6 independent experiments. Statistical analyses were performed by one-way ANOVA followed by Newman Keuls's post-test. **b** Gene expression of glycocalyx markers (*SDC1*: syndecan 1, *SDC2*: syndecan 2, *SDC4*: syndecan 4, *GPC*: glypican, *PLC*: perlecan), as evaluated by qRT-PCR, in HGPS-iPSC SMCs cultured under flow conditions. Gene expression was normalized by the housekeeping gene *GAPDH*, and the normalized gene expression at day 4 divided by day 0. n=3 technical replicates from a pool of 3 independent experiments. **c** HGPS-iPSCs-SMC cultured under flow condition were treated or not with

heparinase III and the number of cells per microfluidic area during culture was calculated and normalized by the number of cells present at day 2. n=3 independent experiments. Statistical analyses were performed by a two-tailed unpaired Student's t-test. **d** Quantification of MMP13 activity (cell culture media) by ELISA. Cells were analyzed at day 4 under flow. Fluorescence signal was normalized by cell number and then by control experimental group. n>9 images examined over 6 independent experiments. Statistical analyses were performed by a two-tailed unpaired Student's t-test (**e**) Expression of alkaline phosphatase in HGPS-iPSCs-SMC, normalized by cell number per mm^2, in cells cultured 4 days under flow conditions. Cells were treated or not with heparinase III. n=2 technical replicates over 3 independent experiments. Statistical analyses were performed by a two-tailed unpaired Student's t-test. In **a** to **e**, results are Mean ± SEM. *,**,***,**** denotes statistical significance ($p<0.05$, $p<0.01$, $p<0.001$, $p<0.0001$). **f** Summary of the results.